Comparison of two tungsten–helium interatomic potentials

Li-Fang Wang, Xiaolin Shu,[a] and Guang-Hong Lu
Department of Physics, School of Physics and Nuclear Engineering, Beihang University, Beijing 100191, China

(Received 19 September 2014; accepted 4 December 2014)

We have clarified the performance of two tungsten–helium analytical interatomic potentials, one of which, developed by Li et al., is a bond-order potential, and another, developed by Juslin et al., is a combination of embedded atom method potential and pair potential. Using these two potentials, we have simulated and made a full comparison of formation energy and migration energy of different defects including helium and vacancy, binding energies of helium and vacancy with helium-vacancy cluster, surface energy, as well as melting point, with reference to the corresponding results from the first-principles and experiments.

I. INTRODUCTION

Tungsten is a promising candidate for plasma-facing materials (PFMs) in tokamak fusion reactors, due to its high melting point and good irradiation resistance. As a PFM, however, tungsten will suffer heavy bombardment from the plasma by particles such as hydrogen isotope and helium ions, which can cause damage such as erosion, sputtering, blistering, and so on. In particular, the low solubility of helium atoms in tungsten provides the driving force for helium atoms to cluster with themselves and other defects, which leads to an accumulation of helium-defect clusters and bubble formation. As the mechanism of bubble formation and the effects of helium-defect clusters on properties of tungsten are still not completely understood, it will continue to be a meaningful subject to investigate the helium behavior in tungsten.

Despite many experimental studies,[1–5] computation has been serving as an essential tool to understand the helium behaviors in tungsten. In consideration of time and space scales of simulation of tungsten–helium system, the classic molecular dynamics (MD) simulation is one of the suitable methods to model the behaviors of helium in tungsten. Many researchers focused on simulating the evolution of the tungsten–helium system based on the MD method, including tungsten surface evolution by helium bubble nucleation, growth and rupture,[6] cascades in tungsten–helium system,[7] mechanism of helium cluster formation in tungsten,[8] helium defect interactions and mechanism of helium bubble growth in tungsten,[9] and helium diffusion in tungsten.[10] In these studies, interatomic potentials remain a key factor to affect the results of the simulations. Therefore, clarifying the performance of the interatomic potential for the tungsten–helium system is quite necessary.

At present, mainly two kinds of interatomic potentials have been constructed to describe the tungsten–helium system. One of the potentials is an analytical bond-order potential (BOP) constructed by Li et al. (P-Li)[11] and another is a hybrid type potential developed by Juslin and Wirth (P-Juslin),[12] an embedded-atom method potential is applied to tungsten–tungsten interaction and two pair potentials are applied to tungsten–helium and helium–helium interactions.

BOP is an empirical potential, which was developed mainly by Tersoff,[13] Abell,[14] and Brenner,[15] and the original potential formalism of BOP has been described by Albe et al.[16] In P-Li, Li et al. used a three-body BOP for the tungsten–tungsten and tungsten–helium interactions.[11] However, as the simulation of tungsten–helium system involves radiation damage effects, a special repulsive potential which describes interactions at a very short interatomic distance to handle the ballistic phase of collisions is needed.[17] In such case, the repulsive part of the BOP is modified by

$$V_{\mathrm{mod}}^{\mathrm{R}}(r) = V^{\mathrm{PP}}(r)[1 - F(r)] + V^{\mathrm{R}}(r)F(r) \quad , \qquad (1)$$

where V^{PP} can be the Ziegler-Biersack-Littmark universal repulsive potential or a repulsive pair potential for a dimer determined by the first-principles method, and $F(r)$ is a Fermi function. As for helium–helium interactions, a two-body potential developed by Aziz et al.[18] is used. For the parameters and full form of P-Li, see Ref. 11.

On the other hand, embedded-atom method is a non-pairwise many-body potential, which is generally used in metals. In potential of P-Juslin, Juslin et al. modified the Ackland–Thetford tungsten potential for the tungsten–tungsten interaction and used a screened Coulomb potential to describe the tungsten–helium interaction.[19] Both potentials are joined with the ZBL universal repulsive potential for

Contributing Editor: William J. Weber
[a]Address all correspondence to this author.
e-mail: shuxlin@buaa.edu.cn
DOI: 10.1557/jmr.2014.407

 © Materials Research Society 2015

https://doi.org/10.1557/jmr.2014.407 Published online by Cambridge University Press

short range interactions by a polynomial function. For helium–helium potential, the Beck potential with the short range fit by Morishita is used in P-Juslin. For the parameters and full form of P-Juslin, see Ref. 12.

Both potentials have been used in the simulation of tungsten–helium system.[6,9,10] Despite this, there are still some confusion about the applicability of both potentials, since the difference of performances between the two potentials has not been clarified. To find out the characteristics of each potential performing on the simulation, in this study we make a thorough comparison between P-Li and P-Juslin by modeling various properties of the tungsten–helium system, and related results calculated by first principles are presented as references.

II. SIMULATION METHODOLOGY

The code LAMMPS[20] is used for the MD simulation. Unless otherwise specified, the sizes of simulation systems are $10 \times 10 \times 10$ $a_0{}^3$, where a_0 is the lattice constant of body centered cubic tungsten, and larger sizes of simulation systems were tested to ensure that system properties were not considerably affected by the system size. The periodic boundary is used in three dimensions in all simulation.

In simulation of defect formation energy, the defects were introduced in the corresponding positions and then the system was carefully relaxed to keep the defects from jumping to the ground state position.[12] The defect formation energy is determined by

$$E_{\mathrm{f}} = E_{\mathrm{def}} - E_{\mathrm{ref}}(N - m_{\mathrm{vac}})/N - E_{\mathrm{ref,He}} n_{\mathrm{He}} \quad , \qquad (2)$$

where E_{def} is the total energy of the system with defects, E_{ref} is the total energy of the system without defects, N is the atom number of the system which in this case N equals 2000, and $E_{\mathrm{ref,He}}$ is the cohesive energy of close packed helium.

In simulation of surface energy, we use a $20 \times 20 \times 20$ $a_0{}^3$ simulation box. To get a specific surface, the simulation box is cut transversely into two parts, which are then separated from each other. After that, the whole simulation system was relaxed. The surface energy is determined by

$$E_{\mathrm{s}} = \frac{E_{\mathrm{final}} - E_{\mathrm{initial}}}{2A} \quad , \qquad (3)$$

where E_{final} and E_{initial} are the energy of the final surface system and the original bulk system, respectively, and A is the area of transverse section.

To get the melting temperature, we used a two phase system which was described in details by Li et al.[21]

As for simulating the helium-vacancy (He-V) cluster, the binding energy of a helium atom or a vacancy to a cluster is calculated by

$$E_{\mathrm{b}}(A_1) = E(A_1) + E(A_2) - E(A_1 + A_2) - E_{\mathrm{ref}} \quad , \qquad (4)$$

where $E_{\mathrm{b}}(A_1)$ is the binding energy of A_1 combined to A_2. $E(A_1)$, $E(A_2)$, and $E(A_1 + A_2)$ are the total energy of the system including A_1, A_2, and $A_1 + A_2$, respectively. E_{ref} is the energy of the pure tungsten matrix.

III. RESULTS AND DISCUSSION

A. Tungsten–tungsten potential

First, we simulate the bulk properties of tungsten to examine the tungsten–tungsten potentials. Self-interstitial atom formation energy, vacancy formation energy, vacancy migration energy, surface formation energy, and melting point of a ground-state tungsten are all calculated based on both P-Li and P-Juslin. All results of calculations are compared with the related data from the first-principles simulations. As a reference, we also present some available experimental results. These data are all shown in Table I.

TABLE I. Bulk properties of tungsten from P-Li and P-Juslin, compared with the first-principles results and experimental results. Here, $E_{\mathrm{f,db110}}$, $E_{\mathrm{f,db111}}$, $E_{\mathrm{f,octa}}$, and $E_{\mathrm{f,tet}}$ are the formation energy (eV) of the 110, 111 dumbbell, octahedral, and tetrahedral self-interstitial atoms, respectively. $E_{\mathrm{f,octa}}$, $E_{\mathrm{f}}^{2\mathrm{vac}}(2NN)$, and $E_{\mathrm{m}}^{\mathrm{vac}}$ are the formation energy (eV) of monovacancy, second nearest neighbor divacancy, and migration energy (eV) of monovacancy, respectively. $E_{\mathrm{sf}}(100)$, $E_{\mathrm{sf}}(110)$, and $E_{\mathrm{sf}}(211)$ are the surface energy (eV) of (100), (110), and (211) surface, respectively. T_{m} is the melting temperature (K) of bcc tungsten.

	P-Li	P-Juslin	First principles	Experiment
$E_{\mathrm{f,db110}}$	9.53	10.22	9.84 (Ref. 22), 10.10 (Ref. 23)	...
$E_{\mathrm{f,db111}}$	9.33	9.52	9.548 (Ref. 22), 9.82 (Ref. 23)	9.06 ± 0.63 (Ref. 24)
$E_{\mathrm{f,octa}}$	12.04	10.42	11.68 (Ref. 22), 11.64 (Ref. 23)	...
$E_{\mathrm{f,tet}}$	10.75	10.78	11.05 (Ref. 22), 11.99 (Ref. 23)	...
$E_{\mathrm{f}}^{\mathrm{vac}}$	3.52	3.63	3.56 (Ref. 22), 3.11 (Ref. 23)	3.7 ± 0.2 (Ref. 25)
$E_{\mathrm{f}}^{2\mathrm{vac}}(2NN)$	6.89	6.86	6.93 (Ref. 22)	...
$E_{\mathrm{m}}^{\mathrm{vac}}$	1.8	1.4	1.78 (Ref. 22), 1.66 (Ref. 23)	...
$E_{\mathrm{sf}}(100)$	3.157	2.920	4.635 (Ref. 26)	2.990 (Ref. 27)
$E_{\mathrm{sf}}(110)$	2.321	2.572	4.005 (Ref. 26)	3.22 (Ref. 28)
$E_{\mathrm{sf}}(211)$	2.904	3.034	4.177 (Ref. 26)	...
T_{m}	4650	4250	...	3695

https://doi.org/10.1557/jmr.2014.407 Published online by Cambridge University Press

The results of self-interstitial atom formation energy from both P-Li and P-Juslin agree well with those from the first-principles simulations. And both potentials predict a correct relative stability for different cases of the self-interstitial atom, which is crucial to the whole simulation of tungsten–helium system. The two potentials also have a good performance in calculating vacancy formation energy. However, vacancy migration energy calculated by P-Juslin is 1.40 eV, which is 0.38 eV lower than the first-principles results. The calculation from P-Li is 1.80 eV, which has a great agreement with the first-principles calculation.

With consideration of tungsten as a PFM, the performance of potentials in simulation of surface properties is very important. Therefore, we examine the surface energy of bcc tungsten. We found out that neither P-Li nor P-Juslin has satisfying performance. The surface energy of (100), (110), and (211) surfaces calculated by P-Li is 3.157, 2.321, and 2.904 eV, respectively, showing the same order of relative stability of the surfaces as those from the first-principles calculations. However, these energies are all much lower than the first-principles results, which are considered unacceptable in an accurate simulation. P-Juslin presents a less precise result to the first-principles calculations. The surface energies that P-Juslin predicted are 2.920 eV for (110) surface, 2.572 eV for (100) surface, and 3.034 eV for (211) surface. These results are apparently inconsistent with those from the first-principles calculations, which we regard as a signal that the potential P-Juslin needs to be improved for the simulation of surface properties. Hence, neither P-Li nor P-Juslin could give convincing quantitative results in simulating surface properties of bcc tungsten, despite P-Li gives better surface properties.

The melting points calculated by P-Li and P-Juslin are both several hundred kelvin higher than the experimental results, though P-Juslin presents a closer result. Structure defects in tungsten that is unavoidable in the actual case may be responsible for the simulated inconsistent melting points with the experimental results. Nevertheless, performances of these two potentials in simulating melting points are both considered reliable.

B. Tungsten–helium potential

1. Formation energy and migration energy of helium in tungsten

To verify the tungsten–helium potentials, we calculate the formation energies of interstitial and substitutive helium, and the migration energy of interstitial helium. All of the calculation results are compared with those from the first-principles and experiments, as listed in Table II.

The formation energies of helium at the tetrahedral interstitial site (TIS) and the octahedral interstitial site (OIS) from both P-Li and P-Juslin exhibit a good agreement with the first-principles calculations. In addition, both potentials give the formation energy of substitutive helium as 4.7 eV, which is exactly the number that the first-principles predicted. This suggests that both P-Li and P-Juslin have a great performance in calculating the formation energies of helium in tungsten.

TABLE II. Properties of helium in tungsten from P-Li and P-Juslin, compared with the first-principles results and experimental results. Here, $E^{He}_{f,tet}$, $E^{He}_{f,octa}$, and $E^{He}_{f,s}$ are the formation energies (eV) of helium interstitial atom in the tetrahedral and octahedral sites and substitutional helium atoms, respectively. $E^{He}_{m}(t-t)$ is the migration energy (eV) of helium between two tetrahedral sites, and $E^{He}_{m}(t-o)$ is the migration energy (eV) of helium between tetrahedral and octahedral sites.

	P-Li	P-Juslin	First principles	Experiment
$E^{He}_{f,tet}$	6.21	6.16	6.16 (Ref. 29), 6.14 (Ref. 30)	...
$E^{He}_{f,octa}$	6.39	6.31	6.38 (Ref. 29), 6.37 (Ref. 30)	...
$E^{He}_{f,s}$	4.7	4.71	4.7 (Ref. 29)	...
$E^{He}_{m}(t-t)$	0.02	0.147	0.06 (Ref. 29)	2.4 ± 0.32 (Ref. 31)
$E^{He}_{m}(t-o)$	0.21	0.149	0.23 (Ref. 29)	...

However, P-Li and P-Juslin exhibit different performances on simulating migration energy of helium in bcc tungsten. P-Li presents the migration energy of 0.02 and 0.21 eV via the diffusion paths of TIS–TIS and TIS–OIS–TIS, respectively, while P-Juslin presents the migration energy of 0.147 and 0.149 eV via the diffusion paths of TIS–TIS and TIS–OIS–TIS, respectively. It should be noted that the migration energy of helium between two tetrahedral sites we calculated in this paper based on the P-Juslin is inconsistent with the result that Juslin et al. had presented before, which is 0.21 eV.[12] The reason why this inconsistence appears is still unclear. Nonetheless, according to the present results, P-Li gives much better migration energy results of helium referring to the first-principles results of 0.06 and 0.23 eV.

2. Binding energy of vacancy to the helium-vacancy cluster

Due to the fact that helium prefers to occupy the vacancy site in bcc tungsten, the interaction between helium and vacancy is important for validating the performance of the fitting potentials. We thus calculate the binding energies of a helium atom and a vacancy to the helium-vacancy cluster based on the potentials of P-Li and P-Juslin.

We first calculate the binding energies of single vacancy to the vacancy cluster. The cluster consists of different numbers of helium atoms and vacancies, which range from zero to four. When the number of helium atom in the cluster is zero, as shown in Fig. 1 and Table III with the available first-principles data, the simulation becomes

https://doi.org/10.1557/jmr.2014.407 Published online by Cambridge University Press

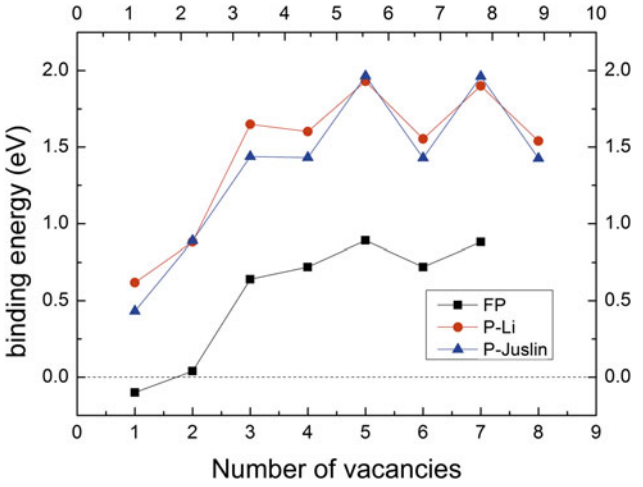


FIG. 1. Binding energy of single vacancy to the vacancy cluster as a function of number of vacancies in the vacancy cluster.

TABLE III. Binding energy (eV) of single vacancy to the vacancy clusters.

Number of vacancies in the clusters	Binding energies		
	FP[32]	P-BOP	P-Juslin
1	−0.1	0.62	0.43
2	0.04	0.88	0.89
3	0.64	1.65	1.44
4	0.72	1.60	1.43
5	0.89	1.93	1.96

a calculation of binding energy of vacancy to the vacancy cluster. Basically, the binding energy from both P-Li and P-Juslin increases with the rising number of vacancies in the cluster and reaches a convergence with some oscillations when the number of vacancies in the cluster is beyond three. This is fully consistent with the changing trends of the first-principles data. However, both P-Li and P-Juslin give higher binding energies from 0.5 to 1.0 eV than those from the first-principles. Furthermore, both P-Li and P-Juslin give positive binding energies, showing the binding preference of vacancy with vacancy cluster, which is slightly different from the results from the first principles. The first-principles give a weak repulsive interaction between two vacancies in tungsten, which exactly the interatomic potentials of both P-Li and P-Juslin fail to reproduce.

With the presence of helium in the cluster, the binding energy of single vacancy to the helium-vacancy cluster behaves differently. As shown in Fig. 2(a), it is found out that, for both P-Li and P-Juslin, the changing trend of the binding energy with the increasing number of vacancies in the helium-vacancy cluster is obviously affected by the number of helium atoms. When the number of vacancies in the cluster is zero, the vacancy exhibits a large positive binding energy with the helium. Such binding energy decreases by 4–6 eV with one more vacancy added in the cluster (Table IV). However, when more than two vacancies are added in the cluster, the variation of binding energy becomes dependent on the number of helium atoms in the cluster. With more than two helium atoms in the cluster, the binding energy of vacancy to the helium-vacancy cluster roughly decreases with the rising number of vacancies in the clusters. But such decrease does not appear when the number of helium atom is less than two.

On the other hand, Fig. 2(b), giving the binding energy as a function of number of helium atoms in the cluster, shows that the binding energy of single vacancy to the helium-vacancy cluster from P-Li and P-Juslin generally increases with the increasing number of helium atoms in the cluster. And the speed of such increase becomes lower when the helium-vacancy cluster contains more vacancies.

Above data agree well with those from the first principles. And they all imply that helium-vacancy clusters with more helium atoms have a stronger attraction to the vacancy, which reveals an attractive interaction between the helium atom and vacancy.

To have a clearer relationship between the binding energy of single vacancy to different sizes of helium-vacancy cluster, we plot the binding energy from P-Li and P-Juslin potential as well as the first principles as a function of ratio between the number of helium atoms and vacancies in the cluster, as shown in Fig. 2(c). The figure presents a nonlinear decrease in the energy that single vacancy binds to the helium-vacancy cluster with an increasing proportion of the numbers of vacancies. In detail, when the ratio of vacancy to helium is less than one (less vacancies than helium atoms in the cluster), the binding energy shows a steep decrease with the increase of the ratio. When the ratio of vacancy to helium is beyond one (more vacancies than helium atoms in the cluster), the decreasing trend of binding energy becomes much slower. Besides, the binding energies of vacancy to the helium-vacancy cluster containing less vacancy than helium atoms are clearly higher than those of vacancy to the clusters containing more vacancy than helium atoms. This again indicates the implication that the helium-vacancy clusters with more helium atoms have a stronger attraction to the vacancy.

All the corresponding data are listed in Table IV.

3. Binding energy of helium to the helium-vacancy cluster

Now we investigate the binding energies of a helium atom to the helium-vacancy cluster containing different number of vacancies (from zero to four) and helium atoms (from zero to five). Figure 3 shows the binding energies of helium to the helium cluster (without vacancy in the cluster) with the available first-principles data, and all

https://doi.org/10.1557/jmr.2014.407 Published online by Cambridge University Press

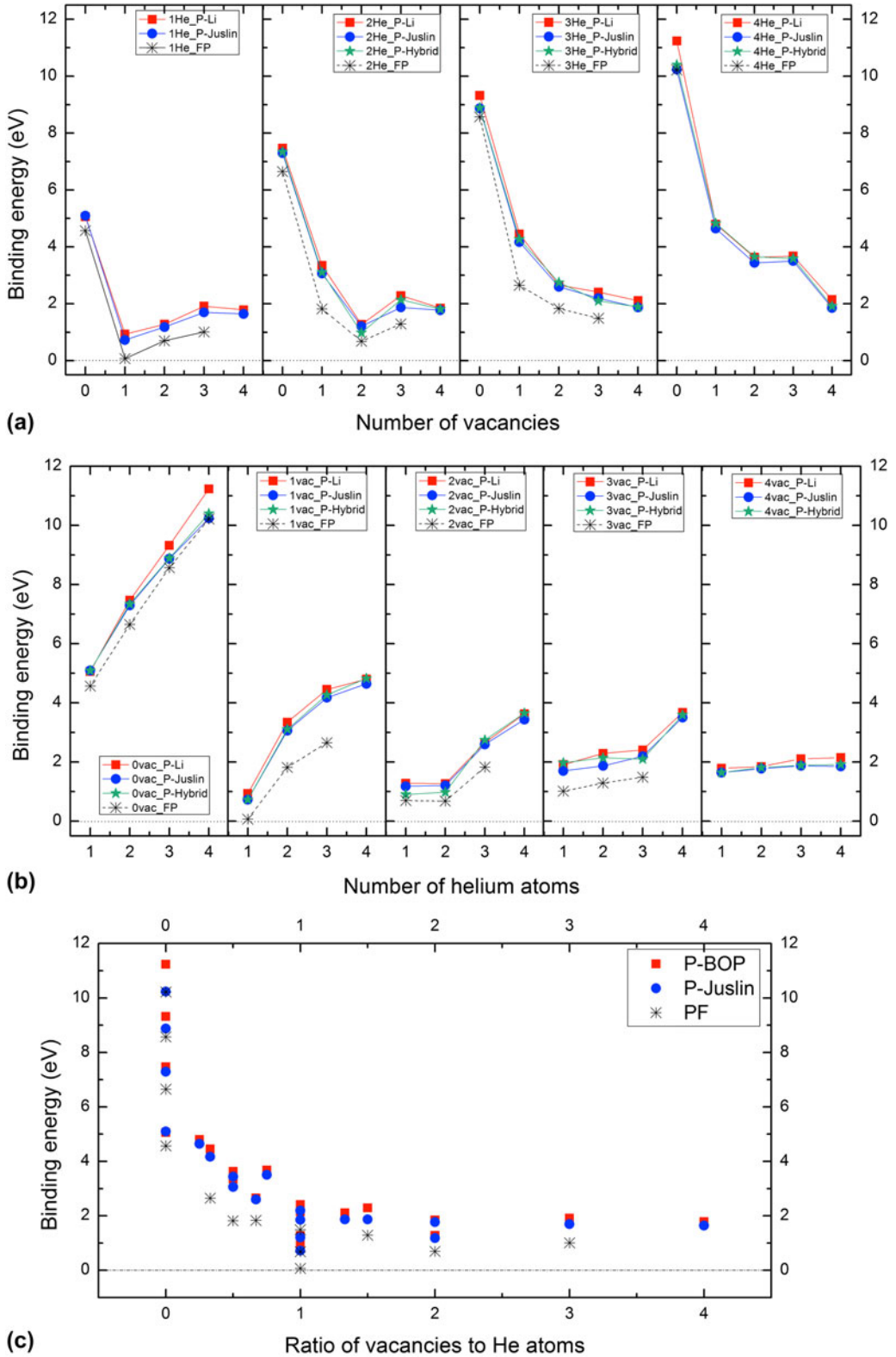


FIG. 2. Binding energy of single vacancy to the helium-vacancy cluster as a function of (a) number of vacancies, (b) number of helium atoms, and (c) ratio between the number of helium atoms and vacancies in the cluster.

the data are listed in Table V. It is found out that both P-Li and P-Juslin potentials give increasing binding energy with increasing number of helium atoms in the cluster, which is consistent with the first-principles results, suggesting a strong attractive interaction and self-trapping characteristics among helium atoms in tungsten.

https://doi.org/10.1557/jmr.2014.407 Published online by Cambridge University Press

TABLE IV. Binding energy (eV) of single vacancy to the helium-vacancy clusters.

Number of vacancies in the clusters	Binding energy (1 helium)				Binding energy (2 helium)			
	FP[32]	P-BOP	P-Juslin	P-Hybrid	FP[32]	P-BOP	P-Juslin	P-Hybrid
0	4.57	5.06	5.09	5.09	6.65	7.47	7.29	7.34
1	0.07	0.93	0.72	0.72	1.82	3.35	3.06	3.11
2	0.7	1.28	1.18	1.18	0.68	1.27	1.21	0.98
3	1.01	1.91	1.70	1.70	1.29	2.29	1.87	2.14
4	...	1.79	1.64	1.64	...	1.84	1.77	1.81
Number of vacancies in the clusters	Binding energy (3 helium)				Binding energy (4 helium)			
0	8.57	9.32	8.87	8.89	10.22	11.24	10.24	10.40
1	2.65	4.45	4.17	4.27	...	4.80	4.64	4.82
2	1.83	2.65	2.60	2.75	...	3.63	3.44	3.65
3	1.49	2.41	2.19	2.10	...	3.68	3.50	3.59
4	...	2.11	1.87	1.89	...	2.15	1.85	1.92

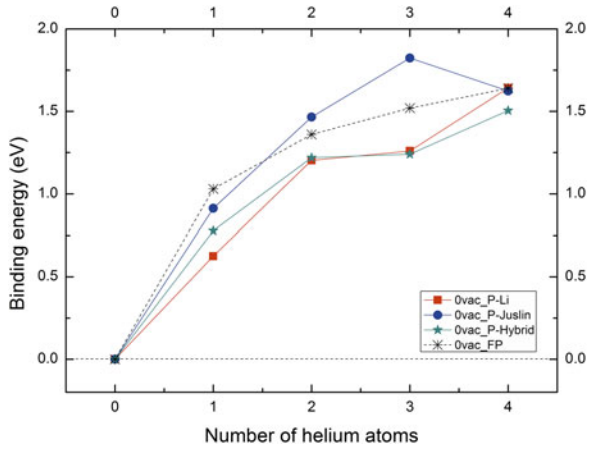


FIG. 3. Binding energy of helium to helium clusters as a function of number of helium atoms in the helium cluster.

TABLE V. Binding energy (eV) of single helium atom to the helium cluster.

Number of helium atoms in the clusters	Binding energies			
	FP[32]	P-BOP	P-Juslin	P-Hybrid
0	0	0	0	0
1	1.03	0.63	0.91	0.78
2	1.36	1.20	1.47	1.22
3	1.52	1.26	1.82	1.24
4	1.64	1.64	1.62	1.50

When vacancy is introduced to the helium-vacancy cluster, the binding energy of helium to the cluster from both P-Li and P-Juslin roughly decreases with the increasing number of helium atoms, as shown in Fig. 4(a). This trend of decrease seems much slower with more vacancies in the cluster. It should be because once there are more vacancies, each helium atom in the cluster has more space. Thus, interaction of helium atom with its neighbor atoms will be weaken, which lowers the variation of the binding energy. In contrast, the binding energy roughly increases with an increasing number of vacancies in the cluster, as shown in Fig. 4(b), reflecting a fact that a helium atom is more easily to bind with the cluster with more vacancies. The relationship of binding energy of helium to the helium-vacancy cluster versus the ratio between number of helium atoms and vacancy in the cluster is also given in Fig. 4(c), which shows a decreasing binding energy of helium to the helium-vacancy cluster with the increasing ratio between numbers of helium and vacancy in the cluster. This again reveals the strong attractive interaction between the helium atom and vacancy.

Besides, these data are also basically consistent with those from the first principles, despite some discrepancies. And all the corresponding data are listed in Tables V and VI.

C. Helium–helium potential

To examine the performance of helium–helium potentials in P-Li and P-Juslin, we switch the helium–helium interaction of P-Juslin by that of P-Li, creating a new combination of W–He potential (P-Hybrid). Thus, the effect of tungsten–helium interaction could be excluded when comparing helium–helium potentials of P-Li and P-Juslin. Furthermore, we could understand how differently two helium–helium potentials could behave in the same tungsten–helium interaction environment by comparing P-Hybrid with P-Juslin, and how differently a helium–helium potential could behave in different tungsten–helium interaction environments by comparing P-Hybrid with P-Li. Binding energies of single vacancy or helium atom to helium-vacancy clusters are calculated to compare these potentials. The calculation results of P-Hybrid are also presented in Figs. 2–4.

https://doi.org/10.1557/jmr.2014.407 Published online by Cambridge University Press

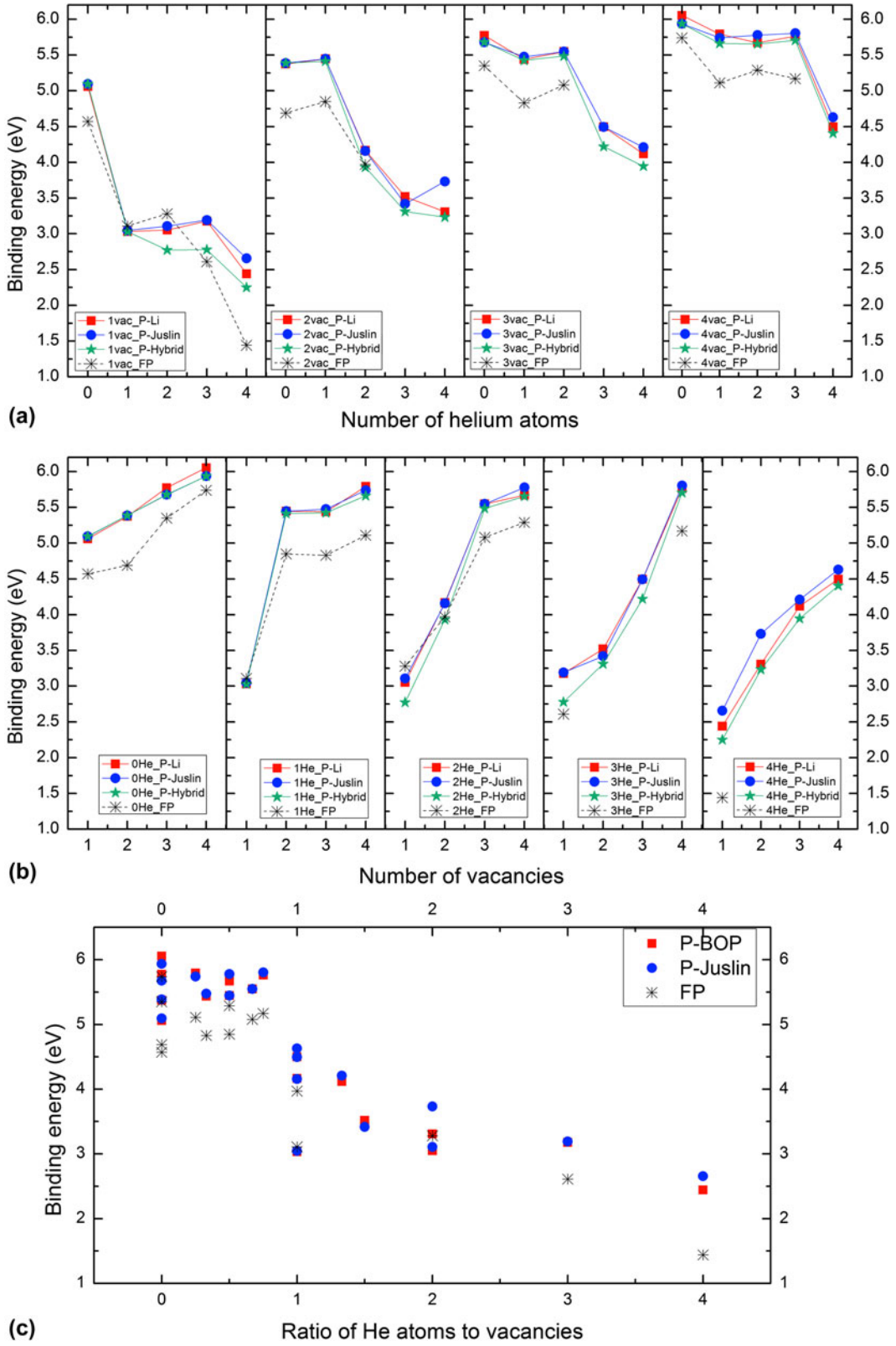


FIG. 4. Binding energy of helium to the helium-vacancy cluster as a function of number of (a) helium atoms and (b) vacancies in the cluster, and (c) ratio between the number of helium atoms and vacancies in the cluster.

https://doi.org/10.1557/jmr.2014.407 Published online by Cambridge University Press

TABLE VI. Binding energy (eV) of single helium atom to the helium-vacancy cluster.

Number of helium atoms in the clusters	Binding energies (1 vacancy)				Binding energies (2 vacancy)			
	FP[32]	P-BOP	P-Juslin	P-Hybrid	FP[32]	P-BOP	P-Juslin	P-Hybrid
0	4.57	5.06	3.05	3.03	4.69	5.37	5.45	5.41
1	3.11	3.03	3.11	2.77	4.85	5.45	4.16	3.93
2	3.28	3.05	3.19	2.78	3.97	4.17	3.42	3.31
3	2.61	3.18	2.66	2.25	...	3.52	3.73	3.23
4	1.44	2.44	3.05	3.03	...	3.31	5.45	5.41
Number of helium atoms in the clusters	Binding energies (3 vacancy)				Binding energies (4 vacancy)			
0	5.35	5.77	5.47	5.43	5.74	6.06	5.74	5.66
1	4.83	5.44	5.55	5.49	5.11	5.79	5.78	5.65
2	5.08	5.55	4.50	4.22	5.29	5.67	5.80	5.71
3	...	4.50	4.21	3.94	5.17	5.76	4.63	4.40
4	...	4.12	5.47	5.43	...	4.50	5.74	5.66

According to Fig. 2, P-Hybrid calculates almost the same binding energies of single vacancy to helium-vacancy clusters as those from P-Juslin. However, according to Figs. 3 and 4, the binding energies of single helium atom to helium-vacancy clusters from P-Hybrid are all slightly lower than those from P-Juslin. This variation becomes much more obvious when the cluster contains more helium atoms. The reason causing such variation is probably that helium–helium potential of P-Hybrid (also P-Li) presents a weaker attractive interaction between helium atoms than that of P-Juslin. So once the system involves considerable helium–helium interaction, its energy is lower based on P-Hybrid than that based on P-Juslin.

Figures 2–4 also show how two different tungsten–helium potentials with the same helium–helium potential affect the binding energies by the comparison of P-Hybrid and P-Li. In these figures, almost all of the binding energies of single vacancy or helium atom to the clusters from P-Hybrid are slightly lower than those from P-Li, which reflects that the tungsten–helium interaction of P-Hybrid (also P-Juslin) is a little stronger than that of P-Li.

Based on the above discussions, it could be concluded that P-Li has a lower interaction between helium atoms than P-Juslin, but such deficiency is offset by its stronger tungsten–helium interaction.

IV. CONCLUSIONS

We have clarified the performance of two tungsten–helium analytical interatomic potentials, one of which is developed by Li et al., with a form of a BOP and another is developed by Juslin et al., with a combination of an embedded atom method and pair potential. Using these two potentials, we have simulated and made a full comparison of formation energy and migration energy of different defects including helium and vacancy, binding energies of helium and vacancy with helium-vacancy cluster, surface energy, as well as melting point, with reference to the corresponding results from the first-principles and experiments.

Both potentials of P-Li and P-Juslin exhibit a reliable performance in simulating the formation energy of defects caused by helium atoms or vacancies. However, P-Li gives a more reasonable migration energy of helium and vacancy than P-Juslin. Neither P-Li nor P-Juslin presents a much satisfying result in the simulation of surface formation energy. In addition, they both predict a consistent changing trend of helium and vacancy binding energy to the helium-vacancy cluster, compared with that from the first-principles calculation. Furthermore, the characters of helium–helium interaction of these two potentials are also clarified by introducing a hybrid potential (P-Hybrid), and we find that P-Li has a slightly weaker interaction between helium atoms than P-Juslin, but such deficiency is offset by its stronger tungsten–helium interaction. According to the above results, overall both P-Li and P-Juslin exhibit a good performance on simulating helium behaviors in tungsten. P-Li gives more accurate energetics due to the characteristics of the three-body potential, while P-Juslin has a much faster simulation speed.

ACKNOWLEDGMENTS

The authors thank Dr. K. Morishita at Institute of Advanced Energy of Kyoto University for offering the full form and parameters of helium–helium potential in P-Juslin. This work is supported by the National Magnetic Confinement Fusion Program through Grant No. 2013GB109002 and the National Natural Science Foundation of China (NSFC) through Grant No. 51171008. G.H. Lu acknowledges support from China National Funds for Distinguished Young Scientists through Grant No. 51325103.

https://doi.org/10.1557/jmr.2014.407 Published online by Cambridge University Press

REFERENCES

1. G-N. Luo, W. Shu, and M. Nishi: Incident energy dependence of blistering at tungsten irradiated by low energy high flux deuterium plasma beams. *J. Nucl. Mater.* **347**(1), 111 (2005).
2. G-N. Luo, W. Shu, and M. Nishi: Influence of blistering on deuterium retention in tungsten irradiated by high flux deuterium 10–100 eV plasmas. *Fusion Eng. Des.* **81**(8), 957 (2006).
3. M. Fukumoto, Y. Ohtsuka, Y. Ueda, M. Taniguchi, M. Kashiwagi, T. Inoue, and K. Sakamoto: Blister formation on tungsten damaged by high energy particle irradiation. *J. Nucl. Mater.* **375**(2), 224 (2008).
4. G-N. Luo, M. Liu, Z. Kuang, X. Zhang, Z. Yang, C. Deng, Z. Zhang, J. Li, and K. Zhou: Directly-cooled VPS-W/Cu limiter and its preliminary results in HT-7. *J. Nucl. Mater.* **363**, 1241 (2007).
5. Y. Ueda, M. Fukumoto, J. Yoshida, Y. Ohtsuka, R. Akiyoshi, H. Iwakiri, and N. Yoshida: Simultaneous irradiation effects of hydrogen and helium ions on tungsten. *J. Nucl. Mater.* **386**, 725 (2009).
6. F. Sefta, K.D. Hammond, N. Juslin, and B.D. Wirth: Tungsten surface evolution by helium bubble nucleation, growth and rupture. *Nucl. Fusion* **53**(7), 073015 (2013).
7. N. Juslin, V. Jansson, and K. Nordlund: Simulation of cascades in tungsten–helium. *Philos. Mag.* **90**(26), 3581 (2010).
8. K.O. Henriksson, K. Nordlund, and J. Keinonen: Molecular dynamics simulations of helium cluster formation in tungsten. *Nucl. Instrum. Methods Phys. Res., Sect. B* **244**(2), 377 (2006).
9. X.C. Li, Y.N. Liu, Y. Yu, G.N. Luo, X.L. Shu, and G.H. Lu: Helium defects interactions and mechanism of helium bubble growth in tungsten: A molecular dynamics simulation. *J. Nucl. Mater.* **451**(1–3), 356 (2014).
10. X.L. Shu, P. Tao, X.C. Li, and Y. Yu: Helium diffusion in tungsten: A molecular dynamics study. *Nucl. Instrum. Methods Phys. Res., Sect. B* **303**, 84 (2013).
11. X-C. Li, X. Shu, Y-N. Liu, Y. Yu, F. Gao, and G-H. Lu: Analytical W–He and H–He interatomic potentials for a W–H–He system. *J. Nucl. Mater.* **426**(1), 31 (2012).
12. N. Juslin and B.D. Wirth: Interatomic potentials for simulation of He bubble formation in W. *J. Nucl. Mater.* **432**(1–3), 61 (2013).
13. J. Tersoff: New empirical approach for the structure and energy of covalent systems. *Phys. Rev. B* **37**(12), 6991 (1988).
14. G. Abell: Empirical chemical pseudopotential theory of molecular and metallic bonding. *Phys. Rev. B* **31**(10), 6184 (1985).
15. D.W. Brenner: Relationship between the embedded-atom method and Tersoff potentials. *Phys. Rev. Lett.* **63**(9), 1022 (1989).
16. K. Albe, K. Nordlund, and R.S. Averback: Modeling the metal-semiconductor interaction: Analytical bond-order potential for platinum-carbon. *Phys. Rev. B* **65**(19), 195124 (2002).
17. K. Nordlund and S.L. Dudarev: Interatomic potentials for simulating radiation damage effects in metals. *C. R. Phys.* **9**(3), 343 (2008).
18. R. Aziz and M. Slaman: An analysis of the ITS-90 relations for the non-ideality of ^{3}He and ^{4}He: Recommended relations based on a new interatomic potential for helium. *Metrologia* **27**(4), 211 (1990).
19. N. Juslin and K. Nordlund: Pair potential for Fe–He. *J. Nucl. Mater.* **382**(2), 143 (2008).
20. S. Plimpton: Fast parallel algorithms for short-range molecular dynamics. *J. Comput. Phys.* **117**(1), 1 (1995).
21. X-C. Li, X. Shu, Y-N. Liu, F. Gao, and G-H. Lu: Modified analytical interatomic potential for a W–H system with defects. *J. Nucl. Mater.* **408**(1), 12 (2011).
22. D. Nguyen-Manh, A.P. Horsfield, and S.L. Dudarev: Self-interstitial atom defects in bcc transition metals: Group-specific trends. *Phys. Rev. B* **73**(2), 020101 (2006).
23. C.S. Becquart and C. Domain: Ab initio calculations about intrinsic point defects and He in W. *Nucl. Instrum. Methods Phys. Res., Sect. B* **255**(1), 23 (2007).
24. I.M. Neklyudov, E.V. Sadanov, G.D. Tolstolutskaja, V.A. Ksenofontov, T.I. Mazilova, and I.M. Mikhailovskij: Interstitial atoms in tungsten: Interaction with free surface and in situ determination of formation energy. *Phys. Rev. B* **78**(11), 115418 (2008).
25. P.M. Derlet, D. Nguyen-Manh, and S.L. Dudarev: Multiscale modeling of crowdion and vacancy defects in body-centered-cubic transition metals. *Phys. Rev. B* **76**(5), 054107 (2007).
26. L. Vitos, A.V. Ruban, H.L. Skriver, and J. Kollár: The surface energy of metals. *Surf. Sci.* **411**(1–2), 186 (1998).
27. W.R. Tyson and W.A. Miller: Surface free energies of solid metals: Estimation from liquid surface tension measurements. *Surf. Sci.* **62**(1), 267 (1977).
28. W. Xu and J.B. Adams: Fourth moment approximation to tight binding: Application to bcc transition metals. *Surf. Sci.* **301**(1–3), 371 (1994).
29. C.S. Becquart and C. Domain: Migration energy of He in W revisited by ab initio calculations. *Phys. Rev. Lett.* **97**(19), 196402 (2006).
30. H.B. Zhou, Y.L. Liu, S. Jin, Y. Zhang, G.N. Luo, and G.H. Lu: Towards suppressing H blistering by investigating the physical origin of the H-He interaction in W. *Nucl. Fusion* **50**(11), 115010 (2010).
31. A. Wagner and D.N. Seidman: Range profiles of 300- and 475-eV He+4 ions and the diffusivity of He4 in tungsten. *Phys. Rev. Lett.* **42**(8), 515 (1979).
32. C.S. Becquart and C. Domain: An object kinetic Monte Carlo simulation of the dynamics of helium and point defects in tungsten. *J. Nucl. Mater.* **385**(2), 223 (2009).

https://doi.org/10.1557/jmr.2014.407 Published online by Cambridge University Press